LWT - Food Science and Technology 77 (2017) 241–248

Contents lists available at ScienceDirect

LWT - Food Science and Technology

journal homepage: www.elsevier.com/locate/lwt

# Non-destructive assessment of the internal quality of intact persimmon using colour and VIS/NIR hyperspectral imaging

Sandra Munera [a, 1], Cristina Besada [b, 1], Nuria Aleixos [c], Pau Talens [d], Alejandra Salvador [b], Da-Wen Sun [e, f], Sergio Cubero [a], José Blasco [a, *]

[a] Centro de Agroingeniería, Instituto Valenciano de Investigaciones Agrarias (IVIA), Ctra. Moncada-Náquera Km 4.5, 46113, Moncada, Valencia, Spain
[b] Centro de Tecnología Postcosecha, Instituto Valenciano de Investigaciones Agrarias (IVIA), Ctra. Moncada-Náquera Km 4.5, 46113, Moncada, Valencia, Spain
[c] Departamento de Ingeniería Gráfica, Universitat Politècnica de València, Camino de Vera, s/n, 46022 Valencia, Spain
[d] Departamento de Tecnología de Alimentos, Universitat Politècnica de València, Camino de Vera, s/n, 46022 Valencia, Spain
[e] School of Food Science and Engineering, South China University of Technology, Guangzhou, 510641, PR China
[f] Food Refrigeration and Computerised Food Technology (FRCFT), Agriculture and Food Science Centre, University College Dublin, National University of Ireland, Belfield, Dublin 4, Ireland

ARTICLE INFO

*Article history:*
Received 30 August 2016
Received in revised form
19 November 2016
Accepted 21 November 2016
Available online 22 November 2016

*Keywords:*
*Diospyros kaki*
Internal fruit quality
Soluble tannins
Astringency
Classification
Computer vision

ABSTRACT

The internal quality of intact persimmon cv. 'Rojo Brillante' was assessed trough visible and near infrared hyperspectral imaging. Fruits at three stages of commercial maturity were exposed to different treatments with $CO_2$ to obtain fruit with different ripeness and level of astringency (soluble tannin content). Spectral and spatial information were used for building classification models to predict ripeness and astringency trough multivariate analysis techniques like linear and quadratic discriminant analysis (LDA and QDA) and support vector machine (SVM). Additionally, flesh firmness was predicted by partial least square regression (PLSR). The full spectrum was used to determine the internal properties and later principal component analysis (PCA) was used to select optimal wavelengths (580, 680 and 1050 nm). The correct classification was above 92% for the three classifiers in the case of ripeness and 95% for QDA in the case of astringency. A value of $R^2 = 0.80$ and a ratio of prediction deviation (RPD) of 1.86 were obtained with the selected wavelengths for the prediction of firmness which demonstrated the potential of hyperspectral imaging as a non-destructive tool in the assessment of the firmness, ripeness state and astringency level of 'Rojo Brillante' persimmon.



## 1. Introduction

Spain is one of the major producers of persimmon (*Diospyros kaki* L.) among European countries (Plaza, Colina, de Ancos, Sanchez-Moreno, & Cano, 2012). The principal variety grown in Spain is 'Rojo Brillante', mostly located in the region of Ribera del Xuquer Valley near Valencia (Spain) with more then 100.000 T per year. This cultivar is very appreciated by consumers because its good aspect, high size, flavour and absence of seeds. However, this cultivar is astringent at harvest and the fruit cannot be consumed until a high degree of overripeness when allowed to rest and soften for a long period after harvest.

This has been traditionally a handicap for the commercialization of this fruit since once the fruit losses the astringency by overripe, it acquires a soft jelly-like consistency being difficult to handle and eat. Now, some methods have been developed to eliminate quickly the astringency without losing the firmness, as exposing fruit to high $CO_2$ concentrations (95–100%) during 18–24 h. This method is based on promoting anaerobic respiration in the fruit, giving rise to an accumulation of acetaldehyde which reacts with the soluble tannins that are the responsible for the astringency (Matsuo, Ito, & Ben-Arie, 1991). In Fig. 1 can be appreciated the differences between a persimmon naturally deastringed by overripeness and another deastringed using a $CO_2$ treatment. Since the success of the treatment was demonstrated (Besada, Salvador, Arnal, & Martínez-Jávega, 2010; Salvador et al., 2007), it has been adopted by industry as the standard deastringency method, and utilized to give the fruit in addition a sweet taste and firm texture similar to the apple, highly appreciated by the consumers. However, the effectiveness

* Corresponding author.
*E-mail address:* blasco_josiva@gva.es (J. Blasco).
[1] These author contributed equally.

http://dx.doi.org/10.1016/j.lwt.2016.11.063
0023-6438/

depends on the fruit firmness at harvest, since maturation process is accompanied by a gradual decrease of firmness (Salvador et al., 2008). A problem is that the stage of maturity at harvest is currently determined based on the visual inspection of experienced growers or using colorimeters due the relationship between the changes in external colour and the internal changes (Salvador, Arnal, Carot, Carvalho, & Jabaloyes, 2006; 2007).

The current way to know the level of astringency in the fruit after $CO_2$-treating is by destructive measurement of soluble tannin content (ST) in random fruits by means of the tannin print method (Matsuo & Ito, 1982) which consists of using a $FeCl_3$-impregnated filter paper to obtain a print of the content and distribution of the tannins trough the reaction with the $FeCl_3$ in the paper. Then, this print is visually assessed by trained workers being this method subjective and destructive and therefore the development of other new non-destructive and accurate methods is needed.

Computer vision systems have been traditionally used to create tools for the objective estimation of the quality of intact fruit production (Cubero, Aleixos, Moltó, Gómez-Sanchis, & Blasco, 2011) and have already been explored to assess quality of persimmon. Mohammadi, Kheiralipour, and Ghasemi-Varnamkhasti (2015) used colour information to determine the maturity of this fruit through colour analysis and classify the fruit into three commercial maturity stages.

Standard computer vision systems tend to mimic the human eye and hence are based on sensors sensible to visible wavelengths. But to analyse internal composition it is necessary the use of technology sensible to non-visible wavelengths related with chemical compounds. This can be achieved by using hyperspectral imaging (Lorente et al., 2012) that is a powerful non-invasive technology that allows obtaining the spatial distribution of the spectral information and it is being used from recent in the internal quality inspection of food (Cheng & Sun 2015; Cheng, Sun, & Cheng, 2016, Cheng, Sun, Pu, & Liu, 2016; Gómez-Sanchis et al., 2013) or to assess some properties of fruits like the ripeness in apples (ElMasry, Wang, Vigneault, Qiao, & ElSayed, 2008), citrus fruits (Folch-Fortuny, Prats-Montalbán, Cubero, Blasco, & Ferrer, 2016), pepper (Schmilovitch et al., 2014), or mango (Vélez-Rivera et al., 2014).

Hyperspectral imaging in persimmon has been used by Munera et al., (2017) to create images showing the distribution of the predicted astringency of each pixel in the fruit, and by Wei, Liu, Qiu, Shao, and He (2014) to predict firmness. However, in this work, the authors claimed that more research is needed to include more samples as well as different regions and different postharvest treatments to ascertain the discrimination power of this method and it is therefore necessary to investigate new methods especially to discriminate among fruits with slightly different stages of maturity or levels of astringency as those exposed to a $CO_2$ treatment, to achieve a demand from both the industry and the consumers. This work proposes a new non-destructive approach based on visible and near infrared (VIS/NIR) hyperspectral imaging and multivariate analysis to determine the firmness, ripeness state and astringency level of intact persimmon 'Rojo Brillante' as alternative to the current destructive and/or subjective techniques.

**Fig. 1.** Persimmon deastringed using a $CO_2$ treatment (left) and persimmon naturally deastringed by overripeness (right). The first shows firm and crisp flesh while the second present a very soft texture.

## 2. Materials and methods

### 2.1. Plant material and internal quality assessments

A total of 90 persimmon (*Diospyros kaki* cv. 'Rojo Brillante') fruits were harvested in L'Alcudia (Valencia, Spain) at three different stages of commercial maturity (M1, M2 and M3) corresponding to different moments of the season (early November, end November, and mid December). A total of 30 fruits, with apparently similar size and colour were collected for each maturity stage. In order to obtain three different levels of astringency, the fruits in each maturity stage were equally divided into three sets. The first set (control fruits with high astringency, HA) consisted of fruits not treated, the second set (medium astringency fruits, MA) consisted of fruits treated in closed containers at 20 °C with 90% of relative humidity (RH) and 95% of $CO_2$ for a period of 12 h, and the remaining set (non astringent fruits, NA) were fruits treated under the same conditions for 24 h.

After each treatment, all the fruits were measured using a colorimeter, a digital camera, and a hyperspectral imaging system. Later, flesh firmness of all fruits was determined by means of a universal testing machine (4301, Instron Engineering Corp., MA, USA) equipped with an 8 mm puncture probe. The crosshead speed during the firmness testing was 10 mm/min. During the test, the force increased smoothly until it drastically decreased when the flesh was broken and the maximum peak force was registered. Results were expressed as the mean of the load (in N) required for breaking the flesh of the fruit on the two sides after peel removal. To analyse the astringency of the fruits, they were sliced and frozen at −20 °C to determine soluble tannins using the Folin-Denis method (Taira, 1995), as described by Arnal and Del Río (2004). This method is based on the reduction of the Folin-Ciocalteu reagent by soluble tannins in alkaline solution. Calibration curve was made with gallic acid. Soluble tannins were extracted by homogenization of 5 g of flesh with 25 mL of 80% methanol solution. Thereafter, samples were filtered and centrifuged for 20 min and the supernatant was reserved. More supernatant was extracted from the precipitant with methanol 80% and added to the first. The supernatant was diluted in water at 1:7 and then Folin-Ciocalteu reagent 1 N was used to conduct the reaction. After 3 min 1 ml of saturated $Na_2CO_3$ was added, and the absorbance of the mixture at 725 nm was measured by colorimetry after stand for 1 h.

### 2.2. Colour analysis

At harvest this fruit presents a uniform colour that ranges from bright to dark orange depending on the maturity being the colour a good indicative of this property (Salvador et al., 2007). The external colour the fruit under study was characterised using two techniques. On the one hand, a colorimeter (CR-300, Konica Minolta Inc, Tokyo, Japan) was used to obtain the colour at three points of the equatorial part of the fruit. Hunter Lab colour coordinates were obtained by the average of three measures. On the other hand, the colour was also evaluated trough images of the two sides of each fruit. The image acquisition system consisted on a digital camera (EOS 550D, Canon Inc, Japan) arranged into a squared inspection chamber that included a calibrated and uniform illumination system composed of eight fluorescent tubes (BIOLUX 18 W/965, 6500 K, Osram GmbH, Germany). The angle between the axis of the lens and the sources of illumination was approximately 45° to avoid direct reflections to the camera (Diago et al., 2015), but due to the spherical shape of the samples these reflections could not be totally avoided this way and hence cross-polarization was also used (ElMasry, Cubero, Moltó, & Blasco, 2012).

A total of 180 images were obtained with a size of 2592 × 1944 pixels and a resolution of 0.11 mm/pixel. Fig. 2 shows examples of images of the fruits in the three maturity stages. For each image, the mean red, green and blue (RGB) colour values of the pixels of the skin were obtained using the application Food_ColorInspector (free download at http://www.cofilab.com). RGB values were later converted to Hunter Lab colour space for analysis using the equations described in Mendoza, Dejmek, and Aguilera (2006) and HunterLab (1996) for illuminant D65 and standard observer 10°. The Hunter Lab coordinates were finally transformed to the colour attributes Hunter luminosity (L), Hunter hue (h) and Hunter chroma (C) (Hutchings, 1999). In addition, RGB values were transformed into HSI (hue, saturation, intensity) values and other indices were estimated such as the ratios $a/b$ and $a/L$ and the colour index ($CI = 1000a/Lb$) (Salvador et al., 2006).

### 2.3. Hyperspectral imaging

Hyperspectral images of the intact persimmons in the spectral range 450–1020 nm were acquired using a camera (CoolSNAP ES, Photometrics, USA) coupled to two liquid crystal tuneable filters (LCTF) (Varispec VIS-07 and NIR-07, Cambridge Research & Instrumentation, Inc., MA, USA). The illumination system consisted of 12 halogen lights arranged equally into a domo inspection chamber where whole fruits were manually introduced (Fig. 3).

Hyperspectral images with a spatial resolution of 0.14 mm/pixel and a spectral resolution of 10 nm were captured in both sides of each fruit (Fig. 4), which lead to a tagged database of 180 hyperspectral images. In each image, a region of interest (ROI) of 225 × 225 pixels in the central part of the fruit was selected and

**Fig. 2.** Images of persimmon at maturity stage M1, M2 and M3 from left to right.

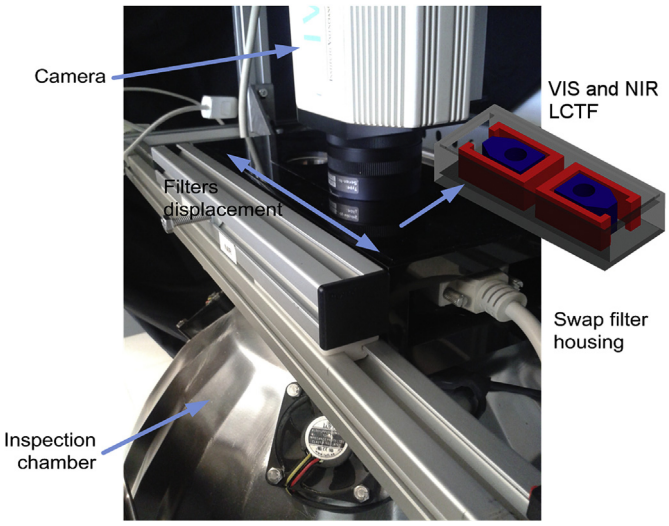


**Fig. 3.** Hyperspectral acquisition system.

analysed as the average of spectrum of all pixels for maturity and firmness analysis since these properties are quite uniformly distributed in the fruit. However, for the case of the astringency, the individual spectrum of each pixel in the ROI was included in the models due the uneven distribution in the fruit of tannins responsible of the astringency. To obtain the relative reflectance of a pixel in the position ($x$,$y$) of the monochromatic band $\lambda$, the original reflectance was corrected using a dark and white reference (Spectralon 99%, Labsphere, Inc, NH, USA) following the procedure described in Gat (2000).

### 2.4. Data analysis

Analysis of variance (ANOVA) and Tukey multiple range test (Statgraphics Centurion XVI - Statpoint Technologies Inc., Virginia, USA) were used to show the effects of ripeness on colour parameters obtained with both, colorimeter and computer vision system. In this analysis, the three maturity stages were the observed values ($Y$) and the Hunter Lab colour coordinates captured by both the colorimeter and the vision systems were the predictive variables.

Hyperspectral images consisted of 67 wavelengths and therefore the spectra obtained from these images were distributed in a matrix with 67 columns each corresponding to the reflectance value of each band where the rows represented the fruits. In addition, the pixels were labelled as belonging to any of the maturity stages (M1, M2 and M3) and treatments (HA, LA, NA) to carry out the analysis for firmness and astringency prediction. First step was a preprocessing of data using Standard Normal Variate (SNV) to remove scatter effects from original spectral data (The Unscrambler X 10.1, CAMO Software, Oslo, Norway). Classification models to sort the fruit by ripeness stage and treatment duration (astringency level) were developed using linear and quadratic discriminant analysis (LDA & QDA), and support vector machine (SVM) (Dutta et al., 2016). The difference between LDA and QDA classifier is that LDA uses pooled covariance to assign an unknown sample to one of the pre-defined groups while QDA uses the covariance of each group instead of pooling them (Naes, Isaksson, Fearn, & Davies, 2002). On the other hand, the SVM algorithm was developed based on the concept of hyperplane and support vectors, using a linear function kernel with C value set to 1. In addition, firmness prediction was conducted by partial least square regression (PLSR) (Cheng et al., 2015b) using the ratio of prediction deviation (RPD), that was defined by Williams (1987) as the ratio of standard deviation of reference values in training set to the root mean square error of prediction (RMSEP).

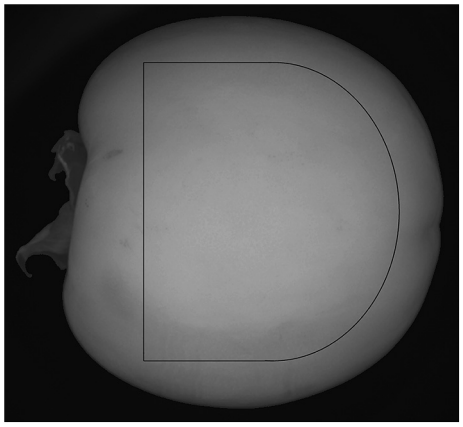

**Fig. 4.** Images of a persimmon (M1) with selected ROI: (a) colour image; hyperspectral image with (b) the VIS filter centred in 640 nm; and with (c) the NIR filter centred in 900 nm.

Hyperspectral systems capture a huge amount of information that is redundant and correlated, especially between contiguous wavelengths (Lorente et al., 2012). Therefore, principal component analysis (PCA) was used to know if it was possible to obtain good prediction using a reduced subset of bands. Four different PCA models were built, one of using the spectral data of the ripeness assessment and the other three PCA with data of the astringency assessment for each harvest. The variables (wavelengths) were chosen on the basis of the size of coefficients or loadings in the eigenvectors of the principal components.

## 3. Results and discussion

### 3.1. Maturity assessment

Several differences can be observed among the spectra of the fruit in the three maturity stages shown in Fig. 5. Fruits of M1 gave higher reflection values than the others in the visible region, which is in agreement with the colour analysis. An absorption peak was found around the bands 670–680 nm only for fruits in M1 stage which could be due the presence of chlorophyll in the more unripe fruit (Lleó, Roger, Herrero-Langreo, Diezma-Iglesias, & Barreiro, 2011). However, the fruits in M2 stage are those which gave a higher reflection in the NIR region that can be due to the chemical differences among fruit at different ripeness. The absorption peak observed around 900–1050 nm could be assigned to water absorption band. This peak was higher in M3, which may be related to water content increases in the flesh during the onset of ripening, which in other fruits has been related to cell breakage and osmotic movement of water from the flesh to the peel.

The PCA model generated with the 67 wavelengths was analysed to identify the variable with the highest factor loadings since they reflected the importance of each wavelength in discriminating differences in the fruit (Wang, Li, Tollner, Gitaitis, & Rains, 2012). The loadings of the first two principal components were used for wavelength selection because these were responsible for 96% of the variance in the spectral data. The wavelengths corresponding to higher module values (peaks and valleys) at these particular principal components were selected as candidates for optimum wavelengths (Rodríguez-Pulido et al., 2013) (Fig. 6). Four optimum wavelengths (450, 580, 680, and 1050 nm) were thus identified for discrimination purposes of different maturity stages. Wavelengths

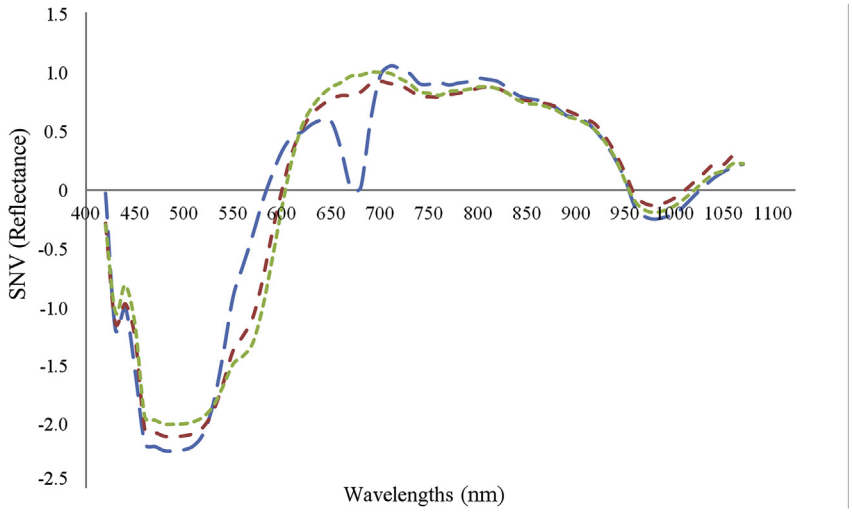


**Fig. 5.** Average spectra of control fruits in three ripeness stages M1 (long dashed line), M2 (medium dashed line) and M3 (short dashed line).

450 nm and 680 nm are related with the presence of beta-carotene and chlorophyll *a* respectively. On the other hand, the importance of the wavelength 580 nm can be due to the colour changes during ripeness since it corresponds to the yellow colour. This would be in accordance with the ranges of h and C values shown in Table 3. The band 1050 nm could be related with an absorption region of water content although the peak is situated below 1000 nm (Lu & Peng, 2006).

Statistical models to classify the fruit into maturity stages were developed using the spectra of the full spectra and only the selected wavelengths. In order to build and validate the model, a 3-fold cross validation procedure was used (Simon, 2007). The data set of pixels was randomly partitioned into three disjoining subsets. The classifier development process was repeated three times using each two different subsets and the resulting classifiers used to classify the remaining test set. Finally the results of the three iterations were averaged.

The four selected bands were used to build the models but also the possible combinations of three bands resulting that using only 580 nm, 680 nm, and 1050 nm, the results were similar to those achieved using the four bands. Using only these three selected wavelengths the success rate of correct classification was slightly lower (mean value of 94.8%) than using the full spectrum (mean value of 98.5%) as shown in Table 1.

Comparing the three classification methods, all of them achieved a good classification above 98% using the all wavelengths. Moreover, using only the three selected wavelengths only LDA showed an important reduction in the success rate while the other two classifiers still remain above 95% which is considered as a good result for a non-destructive technique.

### 3.2. Firmness prediction

Table 2 shows the firmness evolution with the harvesting time (ripeness). A model based on PLSR was built to know if it was possible to predict this property in this cultivar using the wavelengths selected in the previous study for ripeness assessment. For each fruit there was obtained only one global value of the flesh firmness so the prediction model was built using the average values of the pixels selected for each fruit at the determined wavelengths of the hyperspectral images. Cross validation leaving 5% of samples for test was chosen to validate this study. This method splits randomly the data set into the training (95%) and test (5%), repeating the process 20 times. Results were achieved as the mean

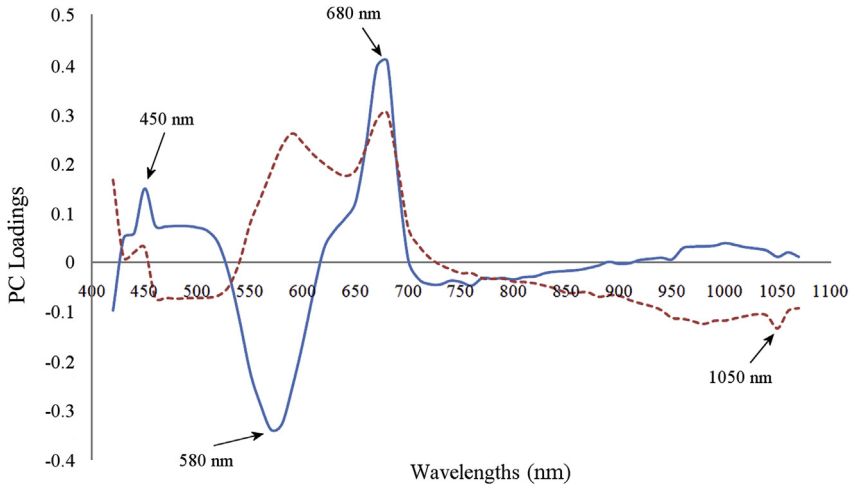


**Fig. 6.** PC Loadings of the PC1 (solid line) and PC2 (dashed line) showing the selected wavelengths for ripeness classification of 'Rojo Brillante' persimmon fruits.

**Table 1**
Ripeness classification of testing set by LDA, QDA and SVM using all and selected wavelengths (cross validation).

| Class | All wavelengths | | | Selected wavelengths | | |
|---|---|---|---|---|---|---|
| | LDA | QDA | SVM | LDA | QDA | SVM |
| M1 | 99.5 ± 0.8$^{a}$ | 99.8 ± 0.4$^{a}$ | 99.1 ± 1.0$^{a}$ | 98.6 ± 0.0$^{a}$ | 99.3 ± 0.7$^{a}$ | 98.4 ± 0.4$^{a}$ |
| M2 | 96.8 ± 3.2$^{a}$ | 96.2 ± 2.9$^{a}$ | 96.0 ± 2.7$^{a}$ | 95.5 ± 2.5$^{a}$ | 94.1 ± 2.2$^{a}$ | 94.7 ± 2.6$^{a}$ |
| M3 | 99.0 ± 0.8$^{a}$ | 100 ± 0.0$^{a}$ | 99.8 ± 0.4$^{a}$ | 83.7 ± 2.3$^{a}$ | 93.9 ± 2.9$^{b}$ | 94.9 ± 1.5$^{b}$ |
| *Total* | 98.5 ± 2.1$^{a}$ | 98.8 ± 2.2$^{a}$ | 98.3 ± 2.3$^{a}$ | 92.6 ± 7.1$^{a}$ | 95.8 ± 3.3$^{a}$ | 96.0 ± 2.4$^{a}$ |

Values are the mean of three models ± standard deviation. Different superscript letters in the same row indicate significant differences between groups (p-value<0.05), according to Tukey's test.

**Table 2**
Flesh firmness (in N) of 'Rojo Brillante' persimmon fruits before and after treatments in the three ripeness stages.

| Group | M1 | M2 | M3 |
|---|---|---|---|
| HA | 47.0$^{a}$ ± 4.3$_{a}$ | 29.0$^{a}$ ± 2.6$_{b}$ | 25.1$^{a}$ ± 3.4$_{c}$ |
| LA | 44.7$^{ab}$ ± 2.6$_{a}$ | 30.9$^{a}$ ± 3.0$_{b}$ | 25.0$^{a}$ ± 4.7$_{c}$ |
| NA | 40.6$^{b}$ ± 2.8$_{a}$ | 31.9$^{a}$ ± 2.1$_{b}$ | 21.1$^{a}$ ± 4.8$_{c}$ |

Values are the flesh firmness (N) ± standard deviation. Different superscript letters in the same column (astringency) and different subscript letters in the same row (ripening) indicate significant differences between groups (p-value<0.05), according to Tukey's test.

of the 20 repetitions.

The coefficient of determination for the prediction ($R^2_P$) was 0.80 and the RPD was 1.86 ± 0.26. Viscarra-Rossel, McGlynn, and McBratney (2006) suggested that calibration models will suffice for good quantitative application if RPD is larger than 1.8. The prediction results obtained was something higher than the minimum proposed but not as good as the prediction results of Wei et al. (2014) for 'Fangshi' persimmon who achieved a $R^2$ value of 0.91. However, in their work the firmness of the fruit ranged from 25 N to 1 N with large differences among the studied classes. In addition, during the ripening process of this cultivar not only drastic changes in firmness happened but also the skin begins to wrinkle and lose shine clearly affecting the reflectance. On the contrary, in the present work, the firmness gave values from 47 N to 21 N which means that these fruits are apparently firm in all maturity stages, which is logical since it is treated to be consumed as firm and crispy fruit. Fig. 1 highlights the visual differences between a soft persimmon naturally deastringed and another deastringed a using $CO_2$ treatment. Hence, for this fruit 80% of prediction capability is considered as a good achievement taking into account the little differences between classes, especially between M2 and M3 classes.

A study was also carried out to analyse the possible correlation between the colour analysis and the firmness of the samples. The characterisation of the external colour was carried out using the colorimeter and the camera only for the control samples of the three stages to avoid the influence of the treatment in colour changes (Table 3). In general, the *L* and *b,* Hunter Lab coordinates, decreased but there were not statistical differences for M2 and M3. On the contrary, the value of *a* increased along the three stages. As a consequence of the changes observed in *a* and *b*, the hue decreased and the chroma slightly increased along the three stages. These differences were observed in the measures given by both, the colorimeter and the camera, and reflect the loss of luminosity of the fruit caused by the maturity process and the changes in the fruit from yellowish-orange to reddish-orange.

The values of the colour attributes (*L*, *h* and *C*) of the colorimeter were higher than the ones obtained from the images. The higher differences were observed for the *L* values since the glossiness leads to a specular reflectance that reduces the contribution to the components *a* and *b*. In fact, colorimeter is very dependent on the scattering properties of the sample while the diffuse illumination of the vision system gives less dependency on the lightness of the sample than the simple illumination and filtering employed by the colorimeter (Trinderup, Dahl, Jensen, Carstensen, & Conradsen, 2015). Despite the differences observed, good correlations where found between the values obtained by both methods ($R^2$ of 0.87, 0.80, and 0.96 for the *L*, chroma, and hue respectively).

Linear regressions were performed between the different colour values, obtained with both the colorimeter and the camera, and the firmness. Tables 4 and 5 summarise the results achieved for the coefficient of determination $R^2$ for each colour component using the imaging system and the colorimeter, respectively. In general, better results are achieved with the imaging system which on the other hand makes sense since they integrate the colour of the whole surface of the fruit while colorimeter only measures in a small spot and thus increasing the variability.

Good correlations are found in *H* ($R^2 = 0.83$), *G* ($R^2 = 0.82$) and *h* ($R^2 = 0.81$) or using simple ratios like *a*/*b* ($R^2 = 0.83$), *G*/*R* ($R^2 = 0.83$) or *a*/*L* ($R^2 = 0.83$). It is worthy of interest that using the simple ratios measured with the imaging system could be obtained better correlations ($R^2 = 0.83$) than using the *CI (CI = 1000a/Lb)* that was the index used by Salvador et al. (2006) to estimate the firmness trough a colorimeter achieving a $R^2 = 0.81$.

### 3.3. Astringency prediction

The results of the measurements of soluble tannins of fresh weight for all maturity stages are shown in Table 6. It can be observed that the tannin content decreased in a similar way for the three maturity stages along with the duration of the treatment. The

**Table 3**
Colour coordinates and attributes of the samples in the three harvests.

| Stage | Colorimeter | | | | | Imaging | | | | |
|---|---|---|---|---|---|---|---|---|---|---|
| | *L* | *a* | *b* | *h* | *C* | *L* | *a* | *b* | *h* | *C* |
| M1 | 58.93 ± 1.83$^{a}$ | 21.71 ± 3.29$^{c}$ | 34.84 ± 1.75$^{a}$ | 60.29 ± 4.41$^{a}$ | 40.67 ± 1.61$^{c}$ | 43.75 ± 1.03$^{a}$ | 27.82 ± 3.54$^{c}$ | 26.03 ± 0.53$^{a}$ | 49.51 ± 4.42$^{a}$ | 36.32 ± 2.00$^{c}$ |
| M2 | 53.49 ± 1.94$^{b}$ | 34.49 ± 1.80$^{b}$ | 31.20 ± 1.41$^{b}$ | 46.46 ± 4.60$^{b}$ | 45.42 ± 1.64$^{b}$ | 33.88 ± 2.44$^{b}$ | 38.30 ± 2.54$^{b}$ | 20.51 ± 1.35$^{b}$ | 34.46 ± 3.78$^{b}$ | 42.07 ± 1.64$^{b}$ |
| M3 | 52.64 ± 1.38$^{b}$ | 38.38 ± 1.65$^{a}$ | 30.77 ± 1.09$^{b}$ | 39.20 ± 1.90$^{c}$ | 48.29 ± 0.53$^{a}$ | 34.71 ± 1.95$^{b}$ | 41.24 ± 1.40$^{a}$ | 21.02 ± 1.05$^{b}$ | 28.62 ± 1.78$^{c}$ | 43.64 ± 1.26$^{a}$ |

Values are the mean of control samples in each harvest± standard deviation. Different superscript letters in the same column indicate significant differences between groups (p-value<0.05), according to Tukey's test.

**Table 4**
Coefficient of determination for the firmness and the different colour components measured with the imaging system.

| | *R* | *G* | *B* | *H* | *S* | *I* | *G/R* |
|---|---|---|---|---|---|---|---|
| $R^2$ | 0.49 | 0.82 | 0.46 | 0.83 | 0.48 | 0.17 | 0.83 |
| | *L* | *a* | *b* | *CI* | *a/b* | *a/L* | *h* | *C* |
| $R^2$ | 0.79 | 0.78 | 0.78 | 0.80 | 0.83 | 0.83 | 0.81 | 0.69 |

R red, G green, B blue, H hue, S saturation, I intensity, L Hunter luminosity, a Hunter a value, b Hunter b value, CI colour index, h Hunter hue, C Hunter chroma.

**Table 5**
Coefficient of determination for the firmness and the different colour components measured with the colorimeter.

| | *L* | *a* | *b* | *CI* | *a/b* | *a/L* | *h* | *C* |
|---|---|---|---|---|---|---|---|---|
| $R^2$ | 0.66 | 0.78 | 0.63 | 0.77 | 0.78 | 0.78 | 0.77 | 0.76 |

L Hunter luminosity, a Hunter a value, b Hunter b value, CI colour index, h Hunter hue, C Hunter chroma.

soluble tannins content decreased to values close to 0.4% in the fruits treated for 12 h to 0.03% in the fruits exposed for 24 h to $CO_2$. Accordingly, Besada et al. (2010) reported that the $CO_2$-treatment applied for 12 h to fruit with firmness around 40 N led to a reduction of soluble tannins to values close 0.3%. Besides, it has been widely reported that a content of soluble tannins of 0.03% after the $CO_2$-treatment is associated with a complete effectiveness of the deastringency process in 'Rojo Brillante' cultivar (Salvador et al., 2007, 2008).

Like in ripeness classification, three PCA models were analysed to identify the highest factor loadings in each ripeness stage. However, no wavelength selection could contribute to the astringency classification. This may be because tannins are mainly detected in the ultraviolet (UV) in the range 190–400 nm (Boulet et al., 2016), or in the NIR (2200–2300 nm) (Cozzolino et al., 2004). For this reason, the whole spectrum in the studied range (450–1020 nm) was necessary to discriminate the astringency.

Table 7 shows the results of astringency classification using the three classifiers. In general, QDA obtained the best overall classification but a reduction of the classification rate along with the maturity was observed, especially for the astringent fruits (HA and LA) in the M3 stage. As it was shown in Table 2, a decrease of firmness in M1 between control and non astringent fruits was observed. However, in M2 and M3 there was no difference. This could be due because the effect of high $CO_2$ concentrations on the cell structure could be the cause of the important loss of firmness observed after deastringency treatment. But when the more ripe samples are treated with $CO_2$, no effect happens on flesh firmness because the loss of intercellular adhesion is already generalised due to the ripeness process (Salvador et al., 2007). Therefore, those changes detected by hyperspectral imaging are assigned to changes in the soluble tannins content and not to changes in texture.

**Table 6**
Soluble tannins content (%) in 'Rojo Brillante' persimmon fruits before and after treatments in the three ripeness stages.

| Group | M1 | M2 | M3 |
|---|---|---|---|
| HA | $0.61^{a} \pm 0.09$ | $0.65^{a} \pm 0.06$ | $0.63^{a} \pm 0.07$ |
| LA | $0.45^{b} \pm 0.04$ | $0.43^{b} \pm 0.10$ | $0.39^{b} \pm 0.06$ |
| NA | $0.03^{c} \pm 0.00$ | $0.03^{c} \pm 0.00$ | $0.03^{c} \pm 0.00$ |

Values are the mean of three measures of soluble tannins content (%) ± standard deviation. Different superscript letters in the same column indicate significant differences between groups (p-value<0.05), according to Tukey's test.

**Table 7**
Astringency classification of test set by LDA, QDA and SVM.

| | Class | Correct classification (%) | | |
|---|---|---|---|---|
| | | LDA | QDA | SVM |
| M1 | HA | $95.9 \pm 0.0^{b}$ | $99.3 \pm 0.0^{a}$ | $97.1 \pm 0.8^{b}$ |
| | LA | $92.4 \pm 4.0^{a}$ | $94.5 \pm 4.3^{a}$ | $94.9 \pm 2.2^{a}$ |
| | NA | $93.9 \pm 2.6^{a}$ | $97.3 \pm 1.5^{a}$ | $93.2 \pm 2.1^{a}$ |
| | Avg | $94.1 \pm 2.8^{a}$ | $97.0 \pm 3.1^{a}$ | $95.1 \pm 2.3^{a}$ |
| M2 | HA | $93.2 \pm 2.5^{a}$ | $96.2 \pm 2.1^{a}$ | $92.7 \pm 1.7^{a}$ |
| | LA | $93.0 \pm 3.4^{a}$ | $95.3 \pm 2.2^{a}$ | $91.1 \pm 3.9^{a}$ |
| | NA | $93.9 \pm 1.1^{a}$ | $95.6 \pm 2.6^{a}$ | $95.9 \pm 1.5^{a}$ |
| | Avg | $93.4 \pm 2.2^{a}$ | $95.7 \pm 2.1^{a}$ | $93.2 \pm 3.1^{a}$ |
| M3 | HA | $83.7 \pm 0.7^{b}$ | $94.3 \pm 1.6^{a}$ | $90.0 \pm 3.4^{a}$ |
| | LA | $72.0 \pm 3.4^{b}$ | $86.0 \pm 3.4^{a}$ | $64.5 \pm 2.2^{b}$ |
| | NA | $93.4 \pm 2.2^{a}$ | $97.3 \pm 1.5^{a}$ | $93.4 \pm 0.7^{a}$ |
| | Avg | $83.0 \pm 9.5^{a}$ | $92.5 \pm 5.5^{a}$ | $82.7 \pm 13.8^{a}$ |
| Overall classification (%) | | $90.2 \pm 7.6^{b}$ | $95.1 \pm 4.1^{a}$ | $90.3 \pm 9.7^{b}$ |

Values are the mean of three models ± standard deviation. Different superscript letters in the same row indicate significant differences between groups (p-value<0.05), according to Tukey's test.

## 4. Conclusions

In this study, VIS/NIR hyperspectral imaging were evaluated as potential non-destructive methods to determine the flesh firmness, maturity stage and the astringency level of 'Rojo Brillante' persimmon.

The characterisation of the colour showed that the *L* and *b*, Hunter Lab coordinates decreased while the value of *a* increased along with the maturity. As a consequence the hue decreased and the chroma slightly increased along the three stages using both colorimeter and image methods. Good correlations were found in some colour parameters like *H* ($R^2 = 0.83$), *G* ($R^2 = 0.82$) and *h* ($R^2 = 0.81$), but also using ratios like *a*/*b* ($R^2 = 0.83$), *G*/*R* ($R^2 = 0.83$) and *a*/*L* ($R^2 = 0.83$) with the data obtained by the imaging system improving previous results. Moreover, better correlations were obtained using these ratios than using the previously proposed CI ($R^2 = 0.80$) which indicates the feasibility of images to assess the colour as a valid alternative to traditional and expensive colorimeters.

Using the hyperspectral system, three wavelengths (580, 680 and 1050 nm) were proposed as the optimum wavelengths for the classification of the fruits into three ripeness stages with high accuracy, more than 94% of all samples were well classified for all of the used classifiers (LDA, QDA and SVM). Moreover, these wavelengths were used for flesh firmness prediction and the RPD value indicated that the obtained model is useful for good quantitative application. Regarding the astringency, the whole spectrum of the fruits needed to be used to classify the fruits into three levels of astringency: astringent fruit, fruit with a low-medium level of astringency and non-astringent fruit. The overall classification for the three ripeness stages was higher than 90% for the three classifiers and higher than 95% for QDA. These results indicate the potential proposed methodology based on hyperspectral imaging as a promising non-destructive tool to assess the internal quality of persimmon fruits destined to be deastringed and rapidly marketed as fresh sweet fruit. However, more research is needed, involving more fruits from different regions and collected in different seasons to ascertain the discrimination power of the proposed

methodology in other markets and conditions.

## Acknowledgements

This work has been partially funded by the INIA and FEDER through projects RTA2012-00062-C04-01, RTA2012-00062-C04-03 and RTA2013-00043-C02, GVA through the project AICO/2015/122, the International S&T Cooperation Programs of China (2015DFA71150), and the International S&T Cooperation Program of Guangdong Province, China (2013B051000010). Sandra Munera thanks INIA for the grant FPI-INIA #43 (CPR2014-0082) partially supported by FSE funds.

## References

Arnal, L., & del Río, M. A. (2004). Quality of persimmon fruit cv. 'Rojo Brillante' during storage at different temperatures. *Spanish Journal of Agricultural Research, 2*, 243–247.

Besada, C., Salvador, A., Arnal, L., & Martínez-Jávega, J. M. (2010). Optimization of the duration of deastringency treatment depending on persimmon maturity. *Acta Horticulturae, 858*, 69–74.

Cheng, J. H., & Sun, D.-W. (2015). Rapid and non-invasive detection of fish microbial spoilage by visible and near infrared hyperspectral imaging and multivariate analysis. *LWT - Food Science and Technology, 62*, 1060–1068.

Cheng, W., Sun, D.-W., & Cheng, J. H. (2016). Pork biogenic amine index (BAI) determination based on chemometric analysis of hyperspectral imaging data. *LWT - Food Science and Technology, 73*, 13–19.

Cheng, W., Sun, D.-W., Pu, H., & Liu, Y. (2016). Integration of spectral and textural data for enhancing hyperspectral prediction of K value in pork meat. *LWT - Food Science and Technology, 72*, 322–329.

Cozzolino, D., Kwiatkowski, M. J., Parker, M., Cynkar, W. U., Dambergs, R. G., Gishen, M., et al. (2004). Prediction of phenolic compounds in red wine fermentations by visible and near infrared spectroscopy. *Analytica Chimica Acta, 513*, 73–80.

Cubero, S., Aleixos, N., Moltó, E., Gómez-Sanchis, J., & Blasco, J. (2011). Advances in machine vision applications for automatic inspection and quality evaluation of fruits and vegetables. *Food and Bioprocess Technology, 4*, 487–504.

Diago, M. P., Tardaguila, J., Aleixos, N., Millan, B., Prats-Montalban, J. M., Cubero, S., et al. (2015). Assessment of cluster yield components by image analysis. *Journal of the Science of Food and Agriculture, 95*, 1274–1282.

Dutta, M. K., Sengar, N., Minhas, N., Sarkar, B., Goon, A., & Banerjee, K. (2016). Image processing based classification of grapes after pesticide exposure. *LWT - Food Science and Technology, 72*, 368–376.

ElMasry, G., Cubero, S., Moltó, E., & Blasco, J. (2012). In-line sorting of irregular potatoes by using automated computer-based machine vision system. *Journal of Food Engineering, 112*, 60–68.

ElMasry, G., Wang, N., Vigneault, C., Qiao, J., & ElSayed, A. (2008). Early detection of apple bruises on different background colors using hyperspectral imaging. *LWT - Food Science and Technology, 41*, 337–345.

Folch-Fortuny, A., Prats-Montalbán, J. M., Cubero, S., Blasco, J., & Ferrer, A. (2016). NIR hyperspectral imaging and N-way PLS-DA models for detection of decay lesions in citrus fruits. *Chemometrics and Intelligent Laboratory Systems, 156*, 241–248.

Gat, N. (2000). *Imaging spectroscopy using tunable filters: A review*. Technical report. Opto-Knowledge Systems Inc. OKSI.

Gómez-Sanchis, J., Blasco, J., Soria-Olivas, E., Lorente, D., Escandell-Montero, P., Martínez-Martínez, J. M., et al. (2013). Hyperspectral LCTF-based system for classification of decay in mandarins caused by *Penicillium digitatum* and *Penicillium italicum* using the most relevant bands and non-linear classifiers. *Postharvest Biology and Technology, 82*, 76–86.

HunterLab. (1996). *Applications note, Hunter Lab color scale*. https://support.hunterlab.com/hc/en-us/article_attachments/201440625/an08_96a2.pdf Accessed November 2016.

Hutchings, J. B. (1999). Food color appearance. In *Food ColorMechanisms* (pp. 453–592). Gaithersburg, Maryland (USA): Aspen Publishers, Inc.

Lleó, L., Roger, J. M., Herrero-Langreo, A., Diezma-Iglesias, B., & Barreiro, P. (2011). Comparison of multispectral indexes extracted from hyperspectral images for the assessment of fruit ripening. *Journal of Food Engineering, 104*, 612–620.

Lorente, D., Aleixos, N., Gómez-Sanchis, J., Cubero, S., García-Navarrete, O. L., & Blasco, J. (2012). Recent advances and applications of hyperspectral imaging for fruit and vegetable quality assessment. *Food and Bioprocess Technology, 5*, 1121–1142.

Lu, R., & Peng, Y. (2006). Hyperspectral Imaging for assessing peach fruit firmness. *Biosystems Engineering, 93*, 161–171.

Matsuo, T., & Ito, S. (1982). A model experiment for de-astringency of persimmon fruit with high carbon dioxide: In vitro gelation of kaki-tannin by reacting with acetaldehyde. *Journal of Agricultural Food Chemistry, 46*, 683–689.

Matsuo, T., Ito, S., & Ben-Arie, R. (1991). A model experiment for elucidating the mechanism of astringency removal in persimmon fruit using respiration inhibitors. *Journal of the Japanese Society for Horticultural Science, 60*, 437–442.

Mendoza, F., Dejmek, P., & Aguilera, J. M. (2006). Calibrated color measurements of agricultural foods using image analysis. *Postharvest Biology and Technology, 41*, 285–295.

Mohammadi, V., Kheiralipour, K., & Ghasemi-Varnamkhasti, M. (2015). Detecting maturity of persimmon fruit based on image processing technique. *Scientia Horticulturae, 184*, 123–128.

Munera, S., Besada, C., Blasco, J., Cubero, S., Salvador, A., Talens, P., et al. (2017). Astringency assessment of persimmon by hyperspectral imaging. *Postharvest Biology and Technology, 125*, 35–41.

Naes, T., Isaksson, T., Fearn, T., & Davies, T. (2002). *A user-friendly guide to multivariate calibration and classification*. Chichester: NIR Publications.

Plaza, L., Colina, C., de Ancos, B., Sanchez-Moreno, C., & Cano, M. P. (2012). Influence of ripening and astringency on carotenoid content of high-pressure treated persimmon fruit (*Diospyros kaki* L.). *Food Chemistry, 130*, 591–597.

Rodríguez-Pulido, F. J., Barbin, D. F., Sun, D.-W., Gordillo, B., González-Miret, M. L., & Heredia, F. J. (2013). Grape seed characterization by NIR hyperspectral imaging. *Postharvest Biology and Technology, 76*, 74–82.

Salvador, A., Arnal, L., Besada, C., Larrea, V., Hernando, I., & Pérez-Munuera, I. (2008). Reduced effectiveness of the treatment for removing astringency in persimmon fruit when stored at 15 °C: Physiological and microstructural study. *Postharvest Biology and Technology, 49*, 340–347.

Salvador, A., Arnal, L., Besada, C., Larrea, V., Quiles, A., & Pérez-Munuera, I. (2007). Physiological and structural changes during ripening and deastringency treatment of persimmon cv. 'Rojo Brillante'. *Postharvest Biology and Technology, 46*, 181–188.

Salvador, A., Arnal, L., Carot, J. M., Carvalho, C., & Jabaloyes, J. M. (2006). Influence of different factors on firmness and color evolution during the storage of persimmon cv. 'Rojo Brillante'. *Journal of Food Science, 71*, 169–175.

Schmilovitch, Z., Ignat, T., Alchanatis, V., Gatker, J., Ostrovsky, V., & Felföldi, J. (2014). Hyperspectral imaging of intact bell peppers. *Biosystems Engineering, 117*, 83–93.

Simon, R. (2007). *Resampling strategies for model assessment and selection chapter 8, pp.173–186 in fundamentals of data mining in genomics and proteomics Dubitzky, Granzow and Berra reds*. NY USA: Springer.

Taira, S. (1995). Astringency in persimmon. In H. F. Linskens, & J. F. Jackson (Eds.), *Fruit analysis* (pp. 97–110). Hannover, Germany: Springer.

Trinderup, C. H., Dahl, A., Jensen, K., Carstensen, J. M., & Conradsen, K. (2015). Comparison of a multispectral vision system and a colorimeter for the assessment of meat color. *Meat Science, 102*, 1–7.

Vélez-Rivera, N., Gómez-Sanchis, J., Chanona-Pérez, J. J., Carrasco, J. J., Millán-Giraldo, M., Lorente, D., et al. (2014). Early detection of mechanical damage in mango using NIR hyperspectral images and machine learning. *Biosystems Engineering, 122*, 91–98.

Viscarra-Rossel, A., McGlynn, R. N., & McBratney, A. B. (2006). Determining the composition of mineral-organic mixes using UV–vis–NIR diffuse reflectance spectroscopy. *Geoderma, 137*, 70–82.

Wang, W., Li, C., Tollner, E. W., Gitaitis, R. D., & Rains, G. C. (2012). Shortwave infrared hyperspectral imaging for detecting sour skin (*Burkholderia cepacia*)-infected onions. *Journal of Food Engineering, 109*, 38–48.

Wei, X., Liu, F., Qiu, Z., Shao, Y., & He, Y. (2014). Ripeness classification of astringent persimmon using hyperspectral imaging technique. *Food and Bioprocess Technology, 7*, 1371–1380.

Williams, P. C. (1987). Variables affecting near-infrared reflectance spectroscopic analysis. In P. Williams, & K. Norris (Eds.), *Near-infrared technology in the agricultural and food industries* (pp. 143–166). St. Paul, MN: American Association of Cereal Chemists.